

SIMULATION OF REACTING AND MOVING GRANULAR ASSEMBLIES OF THERMALLY THICK PARTICLES BY DEM/CFD A BRIEF OVERVIEW

Enric ILLANA², Maximilian BRÖMMER², Siegmund WIRTZ², Viktor SCHERER^{1,2}

¹ Corresponding Author. Tel.: +49 234 / 32-26328. E-mail: scherer@leat.rub.de

² Institute of Energy Plant Technology, Ruhr-University Bochum, Universitätsstraße 150, 44780 Bochum, Germany

ABSTRACT

This paper briefly summarizes the potential and the limitations of the Discrete Element Method (DEM) coupled with Computational Fluid Mechanics (CFD) to simulate chemically reacting, moving granular material passed by fluid flow. A special focus is set on thermally thick particles, which requires to resolve the intra-particle transport and reaction processes. The aspect of complex particle shape is addressed as shape may dominate the particle movement in densely packed granular assemblies even more than details of contact force laws. The fluid flow in the granular assembly is assumed to be a gas, i.e. solid-liquid systems are not considered.

The potential of DEM/CFD will be highlighted presenting three illustrative examples: a large-scale lime shaft kiln with intermittent operation, an industrial-size grate firing system for the incineration of municipal waste, and a small-scale straw pellet stove. In the summary, an outlook is given on open questions and further research needs.

Keywords: Chemical reactions, DEM-CFD, Granular assemblies, Thermally thick particles

NOMENCLATURE

A	$[m^2]$	area
A_g	$[m^2]$	exposed surface
E	$[J]$	total energy
E_y	$[N/m^2]$	Young's modulus
F	$[N]$	force
\underline{J}	$[kg/m^2s]$	diffusion flux of species
M	$[Nm]$	moment
N_S	$[-]$	number of species
R_c	$[K/W]$	thermal constriction resistance
R_g	$[K/W]$	stagnant gas zone resistance
R_i	$[kg/m^3s]$	species production by reaction
T	$[K]$	temperature

S_m	$[kg/m^3s]$	mass source
\underline{S}_{int}	$[kg/m^2s^2]$	interaction force
$S_{i,R}$	$[kg/m^3s]$	species creation from particles
S_P	$[W/m^3]$	heat source from particles
S_R	$[W/m^3]$	heat sources from reaction
Y	$[kg/kg]$	mass fraction of species
g	$[m/s^2]$	gravitational acceleration
h	$[J/kg]$	enthalpy
k^n	$[N/m]$	normal spring stiffness
k^t	$[N/m]$	tangential spring stiffness
k	$[W/mK]$	thermal conductivity
l_g	$[m]$	average distance
m	$[kg]$	mass
\underline{n}	$[-]$	normal vector
p	$[Pa]$	pressure
q	$[W]$	heat transfer
r	$[m]$	radius
r_c	$[m]$	contact radius of contact zone
\underline{t}	$[-]$	tangential vector
v	$[m/s]$	velocity
γ	$[N/m]$	damping coefficient
ε_m	$[-]$	emissivity
θ	$[kg/m^2]$	moment of inertia
θ_{hm}	$[-]$	harmonic mean Poisson's ratio
μ_{dyn}	$[-]$	friction coefficient
ξ	$[m]$	overlap
ρ	$[kg/m^3]$	density
σ	$[W/m^2K^4]$	Stefan-Boltzmann const.
τ	$[N/m^2]$	stress tensor
φ	$[rad/s]$	angular velocity
ψ	$[-]$	porosity

Subscripts and Superscripts

diss	dissipative
eff	effective
el	elastic
f	fluid
g	gas
hm	harmonic mean

n	normal
p	related to the particles
rad	radiation
surf	surface
t	tangential

1. INTRODUCTION

Thermochemical treatment of particles is a core unit operation in process industry. If the particles are large, i.e. must be treated as being thermally thick, this gives rise to additional difficulties in the description. Examples of processes with thermally thick particles are the treatment of minerals in multiple hearth furnaces, the calcination of limestone or magnesite and the reduction of iron oxide by hydrogen in shaft kilns, the production of foamed clay in rotary kilns, the combustion of wood chips or municipal waste on grate firing systems but also the roasting of coffee beans in drum roasters. The difficulty in the description of those kind of systems arises from the facts that:

- particles size is in the cm-range, i.e. particle-internal gradients of temperature and composition must be accounted for,
- with large particles the movement is dominated by shape,
- particles may underlie a particle size distribution leading to segregation,
- particles can change their shape and size,
- phase change (solid-gas) may occur during conversion,
- product quality (calcination degree, reactivity, porosity) depends of the time-temperature history of each individual particle in the reactor.

Virtually always a gas flow is present in the granular assembly. The gas flow can be a gas released by the particles (volatiles from solid fuels, CO₂ from calcination), a gaseous fuel which delivers heat for endothermic particle processes (e.g. calcination) or acts as a reducing media (CO and H₂ in blast furnaces/direct iron ore reduction) or simply air for cooling or combustion purposes.

DEM coupled with CFD is able to describe the above mentioned physical and chemical effects. In DEM, the movement of each particle in a granular assembly is tracked and its interaction with other surrounding particles or walls. Cundall and Strack [1] were the first to introduce DEM for spherical particles in the late 1970s. Considering complex particle shape in DEM is still not standard and is part of ongoing research [2]. Many of the DEM codes like the commercial software Rocky, XDEM, an in-house code of the University of Luxembourg, or LIGGGHTS, a former open source code, can be coupled with CFD. For non-reacting gas-particle system, like fluidized beds, many examples exist for DEM/CFD simulation [3]–[7]. A good overview on non-reacting DEM/CFD including complex particle

shape, particle breakage, attrition and force laws considering adhesion is given by Guo and Curtis [8].

In recent years, chemically reacting systems became of interest in DEM/CFD development. Complexity increases as processes like heat and mass transfer, homogeneous and heterogeneous reactions have to be described in addition. A comprehensive review on heat transfer modelling in DEM/CFD is given by Peng et al. [9] in 2020. An overview on the application of DEM/CFD in process engineering has been presented by Kieckhefen et al. [10] and to chemical process systems by Golshan et al. [11], both in 2020. The last two reviews, however, are mainly limited to small particles (mm-range, thermally thin), with the typical application being fluidized beds. An early overview on the DEM/CFD simulation of thermally thick particles is given by Scherer et al. in 2017 [12].

In our opinion, the real strength of DEM/CFD lies in the description of chemically reacting granular assemblies employing larger particles in the cm-range as intra-particle process can easily be considered in DEM and coupled with the surrounding gas phase. Furthermore, as with size also the mass of the particles becomes large, particle movement is typically dominated by gravitation or mechanical agitation and the influence of fluid flow on the particle movement can be neglected. In addition, the large size of the particles limits particle numbers making the simulation of some industrial-scale systems feasible without employing coarse graining concepts, which cluster a number of particles into parcels, a concept frequently used for fluidized bed simulations [13].

A pioneer in the description of systems with chemically reacting, large particles by DEM/CFD is Peters [14], who presented early work already in the late 1990's. Examples of his current work are the simulation of iron ore reduction in blast furnaces using spherical particles [15] or the combustion of wood pellets, approximating the pellet shape by clustered spheres [16]. He also published a review paper on DEM/CFD which contains further examples [17]. Recently, Gao et al. [18] presented a DEM/CFD study on the pyrolysis of cubic biomass particles using superquadrics for shape representation. Radl et al. [19] presented PARSCALE, an extension to LIGGGHTS, to account for intra-particle heat and mass transfer. They used the oxidation of porous spherical copper particles as an example. In Kuwagi et al. [20], an approach to describe the incineration of nuclear waste (spherical particles) in a fixed bed reactor can be found. A DEM/CFD study on shaft kilns for the production of spinel, using spherical particles, is presented at the current CMFF'22 conference by Spijker and Raupenstrauch [21]. Our own group did use DEM/CFD to simulate the calcination of limestone in shaft kilns [22][23] and the combustion of municipal waste on grate firing systems [24],

where the particles are represented by spheres. The drying of wood chips (cuboids) in a rotary kiln [25] and the combustion of wood pellets (cylinders and spherocylinders) in small-scale heating systems [26], [27] are examples for complex particle shape.

Note that the current brief overview on the simulation of reacting and moving granular assemblies by DEM/CFD can only touch a few specific subjects of thermally thick particles and can't replace the comprehensive reviews mentioned above [8]–[11], [17].

2. METHODS

2.1. Mechanics

In DEM, Newton's Eq. (1) and Euler's equations Eq. (2) describe the translational and rotational movement of particles. The tangential and normal contact forces and moments acting on the particles must be known to solve these equations.

$$\frac{d}{dt} \left(m_i \cdot \frac{dx_i}{dt} \right) = \frac{dm_i}{dt} \cdot \frac{dx_i}{dt} + m_i \cdot \frac{d^2x_i}{dt^2} \quad (1)$$

$$= \sum_{j=1}^N \underline{F}_{ij} + m_i \underline{g} = \underline{F}_i + m_i \underline{g}$$

$$\frac{d}{dt} \left(\theta_i \cdot \frac{d\varphi_i}{dt} \right) = \frac{d\theta_i}{dt} \cdot \frac{d\varphi_i}{dt} + \theta_i \cdot \frac{d^2\varphi_i}{dt^2} \quad (2)$$

$$= \sum_{j=1}^N \underline{M}_{ij} + \underline{M}_i^r = \sum_{j=1}^N \underline{r}_i \times \underline{F}_{ij} + \underline{M}_i^r = \underline{M}_i$$

There are numerous force laws available. An overview is given by Kruggel-Emden et al. for normal [28] and tangential [29] forces. The simplest and still common approach for the normal force is a linear spring-dashpot model [30], where \underline{n} represents the normal vector (Eq. (3)). The first term is the elastic repulsion which is proportional to the overlap ξ between the impacting partners. The second term, the dissipation, is proportional to the normal relative velocity \underline{v}^n . The required contact parameters are the stiffness of a linear spring k^n and the damping coefficient γ^n .

$$\underline{F}^n = \frac{F_{el}^n}{\xi} + \frac{F_{diss}^n}{|\underline{v}^n|} = (-k^n \xi - \gamma^n |\underline{v}^n|) \cdot \underline{n} \quad (3)$$

Eq. (4) gives a typical tangential force law with \underline{t} being the tangential vector, k^t being the tangential stiffness of a linear spring and ξ^t the tangential spring elongation. The force is limited by Coulomb's law.

$$\underline{F}^t = -\min(|k^t \xi^t|, |\mu_{dyn} \underline{F}^n|) \cdot \underline{t} \quad (4)$$

The material parameters are typically derived from single particle measurements and/or are adapted to measurements of static and dynamic angle of repose [31]. For reacting particle systems, the particle surface can get hot and, hence, sticky due to softening or sintering effects, i.e. adequate models for adhesive forces are needed [32]. An example of such force laws is the model introduced by Wissing et al. [24] for municipal waste, where the adhesive force magnitude is based on remaining carbon content in the particle.

The contact time of a collision has to be resolved with a sufficient number of numerical time steps (approx. 20) for a correct temporal description of the evolution of the contact forces. For particles with high elastic modulus, like lime stones or iron ore, this can lead to very short integration time steps and, hence, high computational costs. Therefore, sometimes particles are made artificially softer, i.e. spring stiffness k^n is reduced. This, however, may influence the characteristics of bulk movement but also can alter the gas phase flow field in the packed bed as void spaces among particles change. So far, there is no real universal law how soft particles are allowed to be made and experiments are strongly recommended to check whether DEM with soft particles reproduces the experimental findings. A rule of thumb has been given by Cleary et al. [33] by recommending to limit the maximum overlap ξ_{max} to 0.1 to 0.5 % of the particle radius.

The laws of motion can be integrated by different numerical schemes [34]. For reacting DEM, it is recommended to integrate the product of mass (inertia) and velocity (angular velocity) as mass and inertia may change in parallel with chemical conversion.

In our opinion, contact force models currently seem not to be the bottleneck for reacting DEM as they are able to reproduce the major effects, and this although the force laws are only an approximation of a collision as they do not account for the three dimensional deformation of the particles occurring in reality.

2.2. Particle shape approximation

The major methods to represent particle shape in DEM are depicted in Figure 1. Spheres allow for easy and fast contact detection, and, hence, are sometimes the only solution in case of high particle numbers. The reproduction of the bulk behavior of particles of complex shape by spheres needs an artificial adaption of contact parameters, i.e. the identified contact parameters are then problem specific and can't be transferred to other applications.

Clusters of spheres are the next step of complexity. This approach has the advantage that contact detection still relies on simple algorithms for the collisions of spheres. Cluster of spheres are a good solution as long as just bulk movement is of

interest. However, reacting DEM of large particles requires discretization of the particle interior to account for inner particle processes, which is difficult with clustered spheres. Other methods for particles of complex shape are superellipsoids [35][36] or superquadrics [37][38] which are less computationally demanding than polyhedrons but not as general in shape representation. Polyhedrons (polytopes) allow for the representation of very complex particle shape. Combined with surface triangulation, intra-particle discretization is straightforward. Standard polyhedrons are sharp-edged which very often does not really occur in nature. Therefore, so-called dilated polyhedrons with rounded edges have been suggested by Ji et al. [39] and Desphande et al. [40]. In the very end, it is a problem specific decision which computational effort can be afforded and which details in shape representation is required.

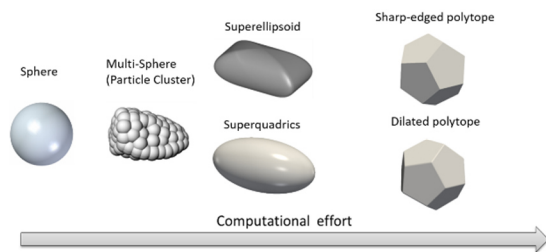


Figure 1. Approximation of particle shape by different methods.

Contact detection in DEM is subdivided into two steps. In a first step, the next neighbors of particles are determined. Fast methods of neighborhood search are hierarchical grids, as used in MercuryDPM [41][42], or octree based approaches [43]. The actual contact detection is the second step and can be very time consuming for complex particle shape. To save computing time, a newer class of contact detection methods pre-computes the relevant parameters of a particle-particle contact (for a given pair of shapes) in dependence of their individual rotation and distance and stores the parameters in a table. Examples are the Orientation Discretization [44] or our own suggestion called Directional Tabulation [40].

2.3. Intra-particle processes

The description of intra-particle processes has to include the diffusive and convective transport of heat and mass as well as source or sink terms for chemical reactions. An overpressure might evolve in the particles due to the generation of a gas within a particle (e.g. volatile release during pyrolysis of wood) [22]. To solve the respective partial differential equations (for brevity not listed here), a discretization of the particle volume is needed. For surface triangulated objects, the discretization is straightforward based on a tetrahedron segmentation.

Other discretization approaches, as cartesian grids or unstructured and non-orthogonal meshes are also possible [45].

For materials which show material anisotropy (e.g. fibrous biomass), 3D particle discretization and the knowledge of directional material parameters are mandatory. An example how important the effect of anisotropy can be, is shown in Figure 2 [46].

The figure shows the simulation of convective drying of silica gel spheres which possess isotropic material properties (left) and beech wood spheres with anisotropic properties (middle and right). For silica gel, the particle shows the highest temperatures in vicinity of the stagnation point, where the highest heat transfer coefficients occur. However, when fiber direction (and moisture transport direction) is parallel to the gas flow, the stagnation point stays cool, as the moisture leaves (and cools) the particle at the stagnation point. As expected, when fiber direction and gas flow are perpendicular to each other, the stagnation point is at higher temperature again.

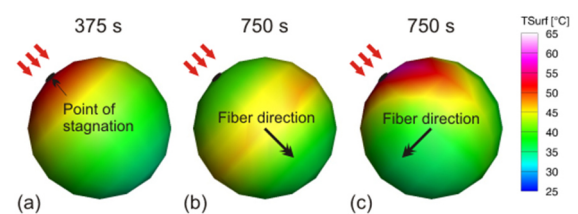


Figure 2. Simulation result for surface temperature: (a) silica gel; (b) beech wood sphere with airflow in fiber direction (c) airflow perpendicular to fiber direction [46].

The complexity of single particle models can vary. For example, drying can be described based on a very simple approach describing just water vapor diffusion or in a more complex manner based on a multi-phase model which resolves the transport of water vapor, free water and bound water [45]. If such complex single particle models as the latter are needed to resolve the underlying physical/chemical effects, single particle models can become a bottleneck in corresponding DEM/CFD simulations.

A remedy can be provided by model reduction. Scherer et al. [25] derived for the anisotropic drying of wood chips spatial modes with corresponding time-dependent coefficients. The coefficients are described by ordinary differential equations. A linear combination of just five modes was sufficient to reproduce the transient solution of the corresponding partial differential equation. A reduction of computing time in the order of 100 could be obtained.

The quality of the single particle model depends on the exact knowledge of physical properties like anisotropic thermal conductivity, diffusion coefficients, permeability or species source terms

like gas release by pyrolysis, parameters which are often not known with sufficient accuracy. Hence, calibration and validation of single particle models by experiments, typically by thermogravimetry, are required (e.g. [45]).

2.4. Contact heat transfer

The appropriate description of contact heat transfer is still a weak point in DEM. To describe contact heat transfer, the contact area must be known. But as contact mechanics in DEM is based on simplified force laws, particle deformation is not really described and, hence, the contact area is not exactly known. For spheres, the approach by Vargas and McCarthy [47] (Eq. (5)) is still very common. Heat is transferred by the direct contact of the two spheres (R_c) and by conduction through the stagnant interstitial gas layer (R_g). The theory of Hertz [48] is used to calculate the contact area between two particles whereby the contact radius r_c of the circular contact zone is utilized to determine the thermal constriction resistance R_c in Eq. (6). For the stagnant gas zone resistance R_g , the exposed surface area A_g of the spheres and average distance l_g between spheres have to be known in Eq. (7). Additionally, care has to be taken to use the real particle stiffness (material parameter) for the calculation of the contact area and not the reduced stiffness often used to solve the equations of motion of the particles.

$$q_{con} = \left(\frac{1}{R_c} + \frac{1}{R_g} \right) \cdot (T_{surf,2} - T_{surf,1}) \quad (5)$$

with

$$R_c = \frac{1}{2 \cdot k_{hm} \cdot r_c} \quad \text{with} \quad (6)$$

$$r_c = \left(\frac{3 \cdot (1 - \theta_{hm}^2) \cdot |F_n| \cdot r_{hm}}{2 \cdot E_{y,hm}} \right)^{\frac{1}{3}}$$

and

$$R_g = \frac{l_g}{k_g \cdot A_g} \quad (7)$$

with $A_g = 2 \cdot \pi \cdot r^2 - \pi \cdot r_c^2$

and $l_g = \frac{r_{hm}^2 \cdot \left(1 - \frac{\pi}{4}\right)}{r_{hm} - r_c}$

As contact heat transfer is also dependent on surface roughness, Tsori et al. [49] present an extension of the approach of Vargas and McCarthy by considering an average slope of particle surface roughness.

The situation gets much more complex for particles of complex shape, as point contacts, line contacts and contacts of planes can occur. A recent suggestion has been made by Joulin et al. [50]

combining DEM with FEM for a realistic modelling of contact area for complex shaped particles. However, easy and fast methods for complex shaped particles to describe contact heat transfer are still missing.

Note that contact heat transfer is important for certain processes as rotary kilns. However, when the granular assembly is passed by a gas very often convection dominates over conduction making an exact knowledge of contact heat transfer less important. The same holds true at high temperature when radiation becomes the dominating effect.

2.5. Radiative heat transfer

For thermally thick, heavy particles, the granular assembly is typically densely packed, i.e. the void spaces among particles are rather small. This allows to neglect gas radiation in the voids as the optical path length is accordingly small.

The most simplest approach to account for bed internal short-range radiation among particle is depicted in Figure 3. This method is based on the assumption that all particles within a volume of radiation influence, the radiation control volume, are in exchange with the target particle. Typically, a control volume of 2-3 particle diameters including the immediate neighbors is sufficient, as this is the approximate viewing distance in a dense bed (at least for granular assemblies with narrow particle size distribution). By this approach, the net heat flux for each particle can be calculated with Eq. (8).

$$q_{rad} = \sigma \cdot \varepsilon_m \cdot A_{surf} \cdot (T_{rad,p}^4 - T_{surf}^4) \quad (8)$$

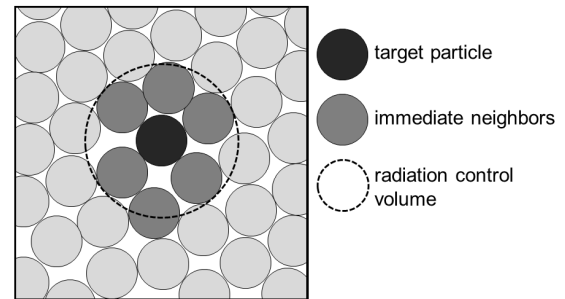


Figure 3. Sketch of the radiation control volume around a target particle [26].

The radiation temperature $T_{rad,p}$ is described by Eq. (9). It is defined as the sum over all emitted heat fluxes of j particles inside the radiation control volume weighted by the surface and emissivity of each particle. This model is highly simplified but fast, especially for moving granular assemblies, and did show reasonable results in comparison with experimental data [51].

$$T_{rad} = \left(\frac{\sum_j \sigma A_j \varepsilon_j T_{S,j}^4}{\sum_j \sigma A_j \varepsilon_j} \right)^{0.25} \quad (9)$$

Note that emissivity ε is often unknown and even can change during a chemical reaction (for example, during decomposition of CaCO_3 to CaO [52]). Hence, appropriate assumptions are needed here.

For a more detailed modelling of radiation exchange between particles, the view factors in all spatial directions from each particle have to be determined. There exist a couple of approaches to derive approximations for the view factors for packings of spherical particles. Methods for monodisperse granular assemblies have been presented by Cheng et al. [53] and Wu et al. [54] and for spherical particle that underlie a particle size distribution by Chen et al. [55]. For monodisperse spheres, an approach has been presented by Forberg and Radl which allows to account for shadowing effects. Finally, Tausendschön and Radl [56] just recently presented a paper on a Deep Neural Network (DNN)-based view factor model to calculate radiative heat transfer between particles. For more detailed insight into these models, we refer to the very good and comprehensive overview on heat transfer modelling in DEM by Peng et al. [9].

The models above assume a uniform temperature of the particle surface of the spheres. Wiese et al. [57] presented an approach to account for particle surface temperature distribution based on surface triangulation.

$$F_{ij} = \frac{\cos \alpha \cos \beta}{\pi |\underline{r}|^2} A_j \quad (10)$$

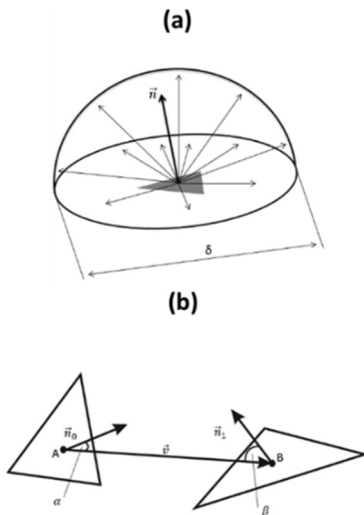


Figure 4. Sketch of the triangle-triangle radiation model [26].

They assumed that every single triangle exchanges thermal radiation with the particles (triangles) in its associated hemisphere (Figure 4a).

In addition, the influence of the distance and the orientation of the triangles (Figure 4b) are taken into account by simplified view factors (Eq. (10)).

Figure 5 shows a DEM-simulation using the triangle-triangle radiation model. The bed consisting of cylindrical pellets is heated up by a hot cylindrical wall surrounding the bed (not shown in Figure 5). Temperature gradients on the particles are clearly visible.

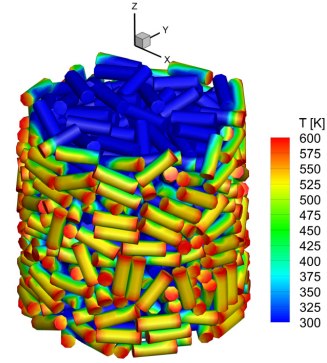


Figure 5. Surface temperature of pellets. The particle bed is heated up by a surrounding cylinder (not shown in the figure) at a radiation temperature of 923 K [57].

The view factor approaches are very helpful, but for moving granular assemblies difficult to handle because view factors must be continuously updated which increases the numerical effort. In addition, for granular assemblies with a wide particle size distribution, the number of surrounding neighboring particles can get very large. Effective, simple models are missing here.

2.6. Particle-Fluid coupling

For the coupling of DEM with CFD, two basic approaches are common. First, a so-called non-resolved DEM/CFD where the particles on the CFD side are just represented by a porosity distribution, i.e. the gas phase is not aware of the details of the particle shape. Typically, the CFD cell size is in the same order of magnitude as the particle size. Second, the flow field around each particle is fully resolved, which leads to CFD cell sizes well below the particle size.

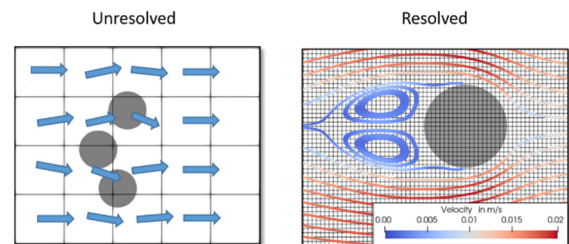


Figure 6. Possible approaches for a gas flow around a particle: (a) Simplified approach with a coarse CFD mesh and a porous medium. (b) Fully resolved flow field around the particle.

The first, unresolved approach is the method of choice or even the only method with affordable computing times for large-scale systems with many particles. The partial differential equations (mass, momentum, species, energy) for the gas phase are based on a porous media approach:

$$\frac{\partial}{\partial t}(\psi \rho_f) + \nabla \cdot (\psi \rho_f \underline{u}_f) = S_m \quad (11)$$

$$\begin{aligned} \frac{\partial}{\partial t}(\psi \rho_f \underline{u}_f) + \nabla \cdot (\psi \rho_f \underline{u}_f \underline{u}_f) = \\ -\psi \nabla p + \nabla \cdot (\psi \underline{\tau}) + \psi \rho_f \underline{g} - S_{\text{int}} \end{aligned} \quad (12)$$

$$\begin{aligned} \frac{\partial}{\partial t}(\psi \rho_f Y_i) + \nabla \cdot (\psi \rho_f \underline{u}_f Y_i) = \\ -\nabla \cdot (\psi \underline{J}_i) + R_i + S_{i,R} \quad i \in [1, N_S] \end{aligned} \quad (13)$$

$$\begin{aligned} \frac{\partial}{\partial t}(\psi \rho_f E_f) + \nabla \cdot (\psi \underline{u}_f (\rho_f E_f + p)) = \\ \nabla \cdot (\psi k_{\text{eff}} \nabla T_f + (\underline{\tau} \cdot (\psi \underline{u}_f))) + S_R + S_P \end{aligned} \quad (14)$$

As shown in Eq. (11) to (14), the coupling between granular and gas phase is primarily based on porosity or void space ψ . The porosity, which varies in space and time for moving granular assemblies, is calculated by DEM and transferred to the gas phase. As the gas phase is not aware of the details of the particle geometry, heat and mass transfer have to be described by Nu, respectively, Sh number correlations. Similarly, momentum transfer (e.g. pressure drop) is represented by correlations, such as the approaches of Ergun [58] and Di Felice [59]. These correlations are reliable for spherical particles, but respective correlations for non-spherical particles are still a topic for ongoing research [60][61][62]. Eq. (13) and (14) also contain source terms to account for chemical reactions, which have to be described by respective models. For gas phase conversion, many models such as Eddy Break Up, Eddy Dissipation Model, Eddy Dissipation Concept or Flamelets exist and can be applied in DEM/CFD. Here, it is more the question how these models, typically reliable or flame propagation in larger combustion chambers, can be applied to the conditions in the tiny void spaces of granular assemblies, where catalytic and/or wall-quenching effects are present and the development of large-scale turbulence structures is suppressed by the length scales of the voids. In addition, for most of the above mentioned models, the reaction progress is based on fuel-oxidizer mixing, but as the flow field is not fully resolved in the porous media approach this puts limitations on the accuracy of the description of gas phase conversion.

For resolved DEM/CFD, immersed boundary methods (IBM) are common. An example is presented at the CMFF'22 by van Wachem et al. [63]. IBM allows for the resolution of particle shape on the fluid-side and, hence, resolution of local flow structures and the associated transfer processes without continuous remeshing as necessary for body fitted CFD simulations of moving particle assemblies. However, although the IBM method is quite powerful, it sets limitations to the number of particles which can be handled due to computational costs., i.e. for large-scale industrial systems the application of IBM is at least critical.

However, in many industrial applications of full resolution of the whole reactor domain is often not required. For example, the lime shaft kiln presented in section 3.1 can be simulated by the non-resolved porous media approach with good accuracy with the exception of the area where gaseous fuel jets enter the packing of lime stones. In this area, a locally resolved simulation would be very helpful as fuel jet penetration and local fuel conversion dominate the temperature field in the reactor (and hence conversion of lime stone to CaO). Therefore, a combination of resolved and unresolved DEM/CFD simulation in one computational domain would be a good solution. Such an approach is suggested by Illana et al. at the current CMFF'22 [64], by using the so-called blocked-off (BO) approach of Patankar [68] for local resolution. The BO method enforces artificial boundary conditions within a static mesh and appropriately blocks the control volumes (CVs) partially or fully obstructed by the boundaries of steady or moving objects. The respective CVs are dynamically identified and excluded from the solution by linearizing the source terms in the discretised transport equations of a CFD solver. For more detail see [64].

The BO method has been applied to an experimental jet in a crossflow setup from literature [65] which is sketched in Figure 7. Particle diameter is 52 mm and the immersion depth of the lance into the bed is 156 mm. The experiments were performed by introducing nitrogen through the lance into the vertically passing laminar air flow. The concentration of oxygen in the passing airflow is obtained as a measure of the gas mixing. For this arrangement, a simulation with the non-resolved porous media approach has been carried out and a simulation where the near-field of the lance has been resolved by the BO method (for details see [64]).

In Figure 8, the concentrations profiles of oxygen obtained from the two approaches at a height of 0.468 m above the lance axis, i.e. a line along the x direction in the vertical cut, are compared with the measurements. It can be observed that the use of the porous media approach results in low O₂ concentrations due to the reduced mixing of the nitrogen flow with the vertical airflow, while the locally resolved approach is able to reproduce the

oxygen concentration level obtained in the measurements. Assuming the N_2 jet would be a gaseous field such an under-prediction of mixing by the porous media approach would of course drastically influence the local heat release by combustion and, as a consequence, the gas phase temperature field and the corresponding local progress of calcination.

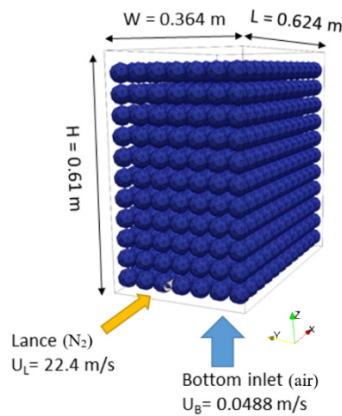


Figure 7. Arrangement of spheres (simple cubic packing) and location of the lance [64].

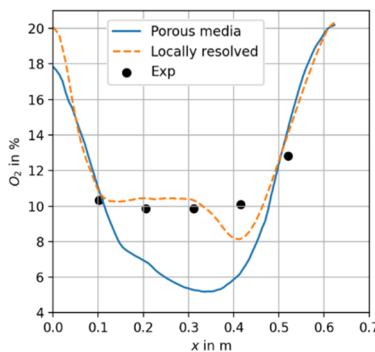


Figure 8. Oxygen concentration profiles at a line located 0.468 m above the lance [64].

Note that at the current CMFF'22 Spijker and Raupenstrauch present a simplified approach, called volume smoother approach, to provide more realistic structure of the particle bed on the CFD side. This approach shifts/smears the volume fraction in the CFD grid to neighbouring cells until a certain threshold. For more details, see [21].

3. SIMULATION EXAMPLES

In the following, three examples of DEM/CFD simulations of a reacting granular assembly with thermally thick particles are presented. First, a lime shaft kiln for the production of CaO from $CaCO_3$, second, a grate firing system for the incineration of municipal waste and third, a straw pellet stove. Whereas in the first two examples the particles are represented as spheres, in the third example spherocylinders are used for pellet shape approximation. In

addition, in the first two examples non-resolved DEM/CFD simulations with the porous media approach were carried out. In contrast, the last example shows a resolved DEM/CFD simulation using the blocked-off approach to represent the particles in the fluid flow. We have taken the three examples from our own group, but of course further important work on DEM/CFD simulation of reacting thermally thick particles have been carried out by others (e.g. [14]–[16], [18]–[21]). Note that the simulations presented here were carried out with our in-house code called LEAT-DEM coupled with FLUENT.

3.1. Lime shaft kiln

In the calcination process, limestone is converted at high temperatures ($T > 900$ °C) into calcium oxide and carbon dioxide. The current example is based on a so-called parallel-flow regenerative lime shaft kiln (PFR-kiln) [66]. The example is based on an existing industrial kiln, part of the product portfolio of the Maerz Ofenbau AG, Switzerland. A PFR-kiln consists of two vertical shafts and a connecting crossover channel (see Figure 9). The lime stones move through the shafts due to gravitation. While in one shaft the calcination takes place in parallel flow of particles (the necessary heat is provided by the combustion of methane), the other shaft preheats the lime stone in counter flow. It is a transient process since the two shafts periodically switch their function at cycles of 15 min. Due to the regenerative process, PFR-kilns show the lowest heat consumption of lime kilns available today.

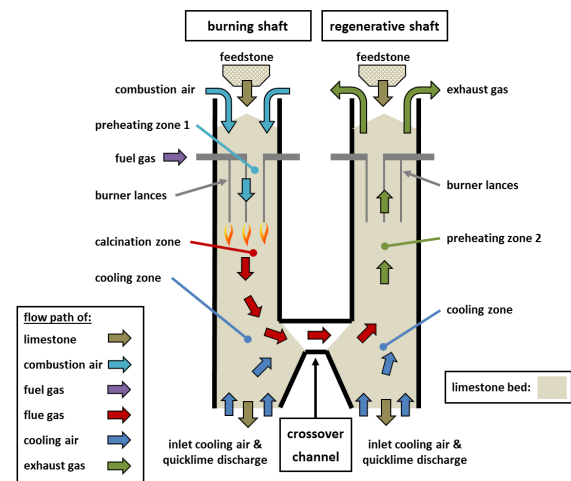


Figure 9. Operation principle of a rectangular PFR-kiln – gas flow and limestone movement [66].

In the simulation, contact heat transfer, radiative heat transfer among particles and convective heat transfer are considered. The single particle calcination model includes diffusion and advection (Stefan flow) of CO_2 . Gas phase combustion of

methane is considered by a two-step mechanism including the intermediate formation of CO. The lime stones, represented by spheres, underlie a particle size distribution (50-90 mm). The total height of a single shaft is 18 m, and its width is 1.6 m. The end of the burner lances is 5.8 m below the limestone inlet.

Figure 10 shows the gas temperature and CH₄ mass fraction at the end of one cycle in the plane of symmetry. The left shaft is the burning shaft. The highest temperature occurs close to the burner lances where the methane is combusted. The heat of calcination act as a heat sink and, therefore, areas of higher temperatures diminish fast. Gas temperature in the calcination zone of the burning shaft is between 1000 °C and 1200 °C. In the right shaft, the regenerative shaft, the maximum temperature is around 900 °C. The right image shows the mass fraction of methane. Methane is converted just before the exhaust gases reach the crossover channel. A too long flame is undesired as combustion in the crossover channel would generate high temperatures possibly damaging the refractory lining in that area.

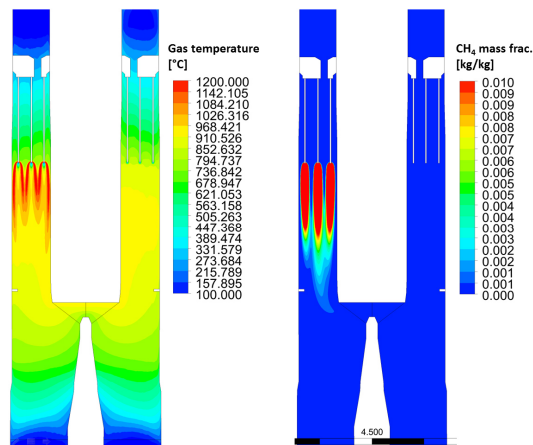


Figure 10. Fluid temperature and CH₄ mass fraction in the fluid phase (plane of symmetry). Results taken from the CFD-simulation at the end of one cycle. The left shaft represents the burning shaft [66].

Figure 11 left shows the particle residence times. The mean residence is about 20 h and identical in burning and regenerative shaft. The particles near the inner cooling zone wall have longer residence times caused by the shaft slope. In the upper shaft, the radial residence time distribution shows almost no gradients, i.e. no core flow exists. The second image shows the degree of calcination of each individual particle. Smaller particles are completely calcined, whereas larger particles show a lower degree of conversion. Furthermore, the kiln operates with a reduced conversion efficiency near the outer wall, because the hot flue gas flows towards the crossover channel and thus closer to the inner wall. In total, the mass averaged calcination degree of the exiting

limestone is about 95 %. Note that industrial PFR-kilns operates at conversion degrees over 99.9 %, which could be achieved in the simulations too by increasing the thermal input.

In the paper [66], we also show a comparison with temperature measurements. A thermocouple lance was used, which travels with the limestone bed through the kiln. Agreement was fair, keeping in mind that just a single thermocouple reading was available in the large kiln. This also highlights an important research need for further work. Measurement is such in kind of high temperature reactors are scarce and extremely challenging. However, for DEM/CFD calibration such data are urgently needed.

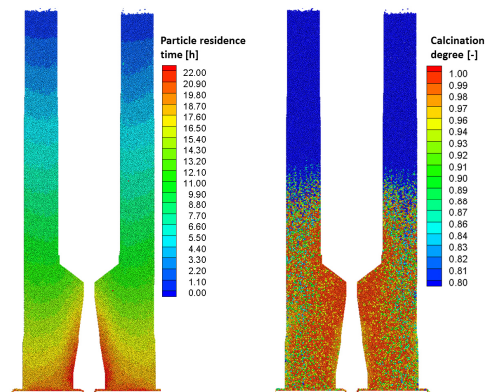


Figure 11. Particle residence times and calcination degrees (plane of symmetry). Results taken from the DEM-simulation at the end of one cycle. The left shaft represents the burning shaft [66].

3.2. Waste incineration plant

The second example is based on municipal waste incineration plant in Germany [24]. The MHKW Frankfurt has a thermal load of 57 MW_{th}. The grate consists of two sections (see Figure 12, bottom). The first one is inclined by an angle of 10°, has a length of 7.3 m. The second grate section is located 0.54 m below the first section. The length of this horizontally arranged section is 3.06 m, the width of the grate is 7.36 m. To save computing time just a strip of 50 cm width has been simulated. The waste bed is supplied by primary air (in crossflow to the waste bed) through six primary air zones. The waste transport is due to movable (forward-acting) stoking bars. The mean residence time on the grate is approximately 90 minutes. Above the grate, the released volatiles are converted in the combustion chamber. Secondary air is injected for conversion of the volatiles in a gas flame. The gas flame exchange radiative with the fuel bed, an important mechanism for waste ignition and conversion.

The waste particles are represented as spheres. Of course, waste particles are not spherical, hence, the sphere dimensions represent the area of

mechanical influence of a specific fuel particle rather than its actual geometry. The fuel is subdivided in up to 11 fractions such as plastics, organics, textiles, sanitary products etc. Each fraction has its own fuel characteristics, i.e. chemical composition, heating value, particle size distribution and, hence, shows different combustion behavior. Maximum particle size is 0.27 m. Drying, pyrolysis and char combustion and gasification are modelled. Pyrolysis gas combustion is modelled by a one-step reaction based on a volatile surrogate species. Particle size changes (shrinks) during conversion due to fuel conversion. A model which accounts for adhesive forces is implemented. The adhesive forces become lower with increasing fuel conversion; a linear decrease with remaining fuel carbon content is assumed.

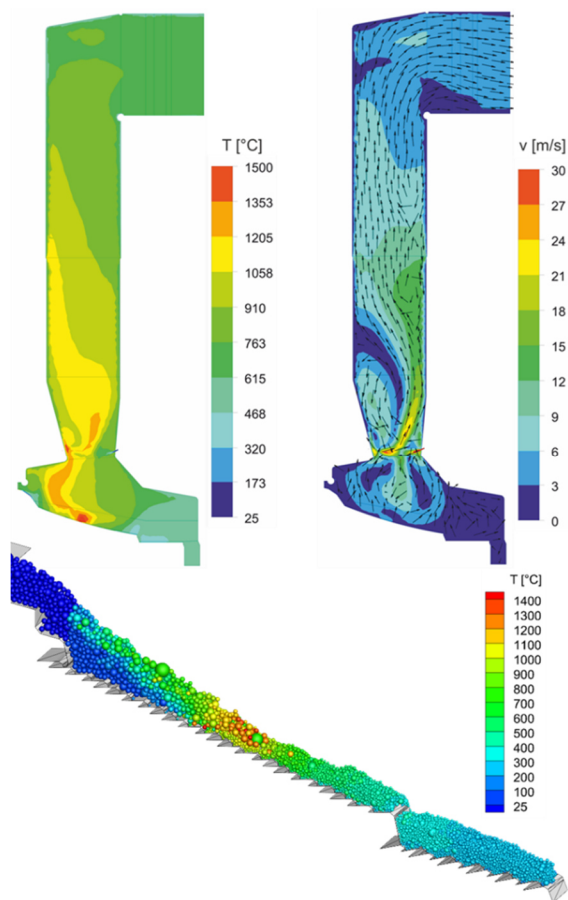


Figure 12. Temperature (top left) and velocity (top right) distribution in the furnace; surface temperature of waste particles (bottom) [24].

Examples of results are shown in Figure 12. The upper figures depict the temperature and velocity distribution of the gases in the symmetry plane of the combustion chamber. The lower figure shows the corresponding particle surface temperature of the waste particles. Waste enters the grate from the left and is transported to the right. The maximum surface temperature of the particles is up to 1400 °C, typically at 50% traveling distance. Further

downstream, with proceeding conversion, the temperature decreases due to cooling by the primary air. The particles leave the grate with temperatures in the order of 200 °C to 300 °C.

The maximum of the gas temperature (top left) reaches its maximum at the same position as the maximum waste temperature. The gas temperature of approx. 1500 °C is 100 °C higher than the waste temperature, which is due to the conversion of CO and volatiles above the waste bed. A temperature asymmetry occurs, as the temperature close to the boiler front wall (left) is higher than the temperature at the back wall (right).

The absolute velocity and the velocity vectors (top right) clearly depict the location of secondary air injection, which is injected from the front and the back wall, inducing strong mixing and a recirculation zone close to the front wall. Downstream of the secondary air injection, a streak can be observed that stretches from the front to the back wall and again to the front wall inducing a recirculation zone at the back wall.

Another important information that can be derived from such simulation is the change in the volume of the waste fraction due to conversion. This is depicted in Figure 13 for the 11 fractions simulated. The largest change in volume occurs for wood (low ash content, high volatile content) and plastics (low ash content, high volatile), whereas the smallest change (with the exception of inerts) can be observed for fines as they contain a large amount of ash.

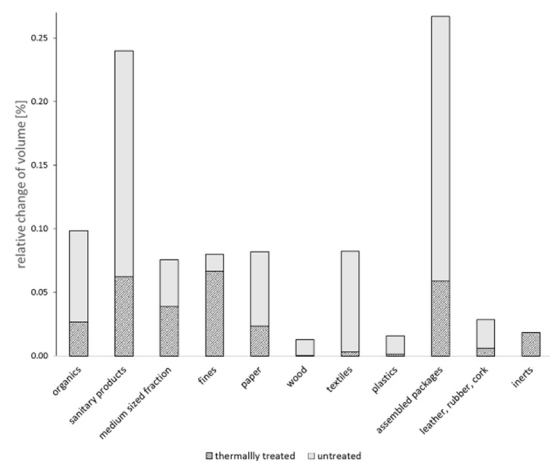


Figure 13. Relative change of volume before and after thermal treatment for the 11 waste fractions considered [24].

3.3. Straw pellet stove

As a last example, a simulation for non-spherical particles is presented with a resolved DEM/CFD approach based on the blocked-off method introduced earlier [27]. The test case is sketched in Figure 14 a. It consists of a cylindrical combustion chamber for gas phase combustion and a cylindrical

burner bowl filled with straw pellets. The wall of the combustion chamber is electrically heated to 1000 K. It provides the radiative heat for pellet ignition. Primary air is passing the fuel bed through the grate located at the burner bowl bottom. Secondary air is added to the combustion chamber above the pellet bed. Primary to secondary air mass flow ratio is set to 20 %. Details of the burner bowl with the grate formed by three stoking rings are shown in Figure 14. The stoking rings allow for mechanical agitation of the pellet bed (see Figure 14 b and c: initial position b, fully traversed stoking rings c). The inner stoking ring as well as the outer stoking ring can be moved vertically. The central element is static. Different stoking pattern can be carried out.

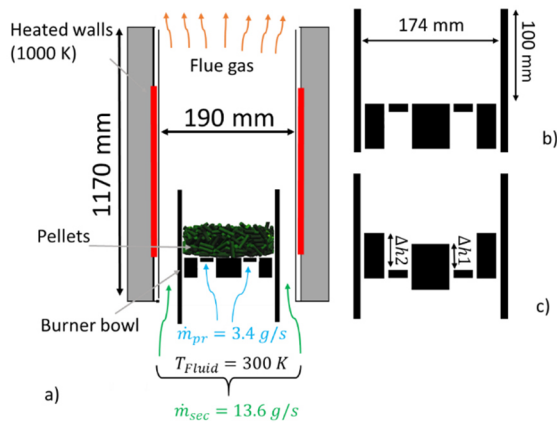


Figure 14. a) Sketch of the test rig, b) static burner bowl and c) burner bowl with fully traversed stoking elements [27].

The particles in the DEM/CFD simulation are represented by surface triangulated spherocylinders. The number of intra-particle cells is in the order of 500. Pellets shrink during volatile release but keep their shape during char burnout (the ash of straw tends to agglomerate and forms a stable skeleton). The pellets underlie a length distribution from 9 to 25 mm. Radiation is modelled by the discrete ordinate model (DOM) which has been combined with the blocked-off method, hence also bed internal radiation is modelled by DOM. To account for the turbulence structure of the gas phase above the bed, very large eddy simulation (VLES) has been applied. The particle reaction model includes drying, pyrolysis and char conversion. Pyrolysis gas combustion is modelled by a two-step reaction based on a pyrolysis gas surrogate and the intermediate formation of CO.

Figure 15 shows the temperatures and water contents of the pellets after 400 s of operation (top static bed, bottom agitated bed). At this moment in time already volatile release occurs, but no volatile flame is present. Thus, the energy supply to the bed occurs due to radiation by the electrically heated combustion chamber walls. In the static case,

particles with high temperatures (top, left) are located in the top layer. Radiative heat from the walls is absorbed at the surface of the pellets but cannot reach pellets in deeper layers. In case of bed agitation, this is considerably different. Here, the number of hot particles at the surface is smaller. This can be explained by the fact that hot pellets from the top layer are transported into the bulk where radiative heat exchange with the heated walls above the burner bowl is blocked and convective cooling of pellets by primary air occurs. For the static mode, the absence of pellet mixing leads to a typical separation layer between raw pellets inside the bed and dry pellets at the bed surface (top, right), whereas for the agitated case pellet mixing leads to a much more homogeneous drying of the bulk.

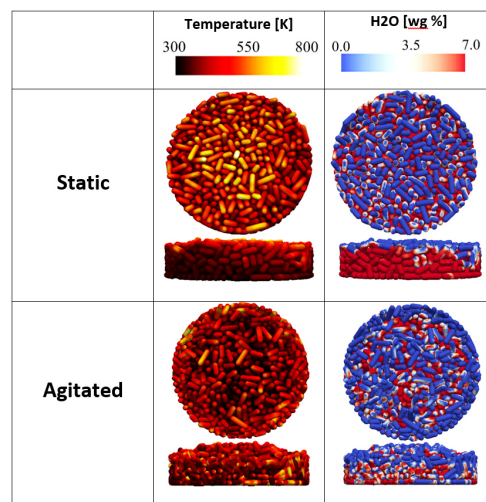


Figure 15. Distribution of temperature and water content in the bulk after 400 s [27].

Figure 16 shows a cross-sectional view through the center of the burner bowl for the static (left) and the agitated (right) operation after 600 s of operation. Merged contour plots of the gas temperatures and temperature distribution inside each individual pellet are depicted at the top in a logarithmic scale. Respective plots of the oxygen mass fraction of the gas phase are shown below.

At this point, a significant amount of volatiles has been released to the gas phase for the static case, leading to a gas flame above of the bed. Therefore, the maximum temperature level is significantly higher compared to the agitated case. Maximum temperatures (1000 K) occur at the bed surface due to conversion of volatiles as well as heterogeneous char combustion at the pellet surface. This leads to regions of lower oxygen mass fractions directly downstream of the fuel bed.

In agitated operation, the temperature level is significantly lower. Mixing of the bulk leads to a homogeneous but overall reduced heating of gas phase and pellets. This leads to less volatile products in the gas phase and only minor consumption of

oxygen by gas phase (no volatile flame present) and heterogeneous char reaction.

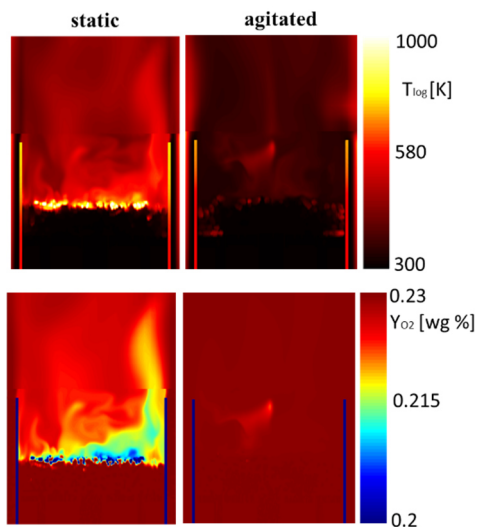


Figure 16. Contours of gas phase temperature and oxygen mass fraction after 600 s for a static bed (left) and an agitated bed (right) [27].

4. SUMMARY AND CONCLUSION

An overview is given on DEM/CFD simulation of reacting and moving granular assemblies passed by gas flow with a focus on thermally thick particles. The approaches to represent complex particle shape, heat and mass transfer, intra-particle process and chemical conversion are briefly summarized. Three examples are presented, namely a large-scale lime shaft kiln with intermittent operation, an industrial-size grate firing system for the incineration of municipal waste, and a small-scale straw pellet stove. These examples demonstrate the deep insight that can be gained by DEM/CFD into the chemical/physical processes in densely packed, chemically reactive granular assemblies with gas flow. For example, DEM/CFD allows for the prediction of particle product quality (e.g. calcination degree in lime shaft kilns) as intra-particle processes are resolved. When complex particle shapes are considered, a realistic description of effects like bridging, arching or segregation in moving granular assemblies is possible, which is very difficult to achieve with continuum approaches.

Despite of these advantages, there are still limitations of DEM/CFD for actual technical systems. Computing time for large-scale systems is still high, especially for particles with complex shape. Therefore, for many large-scale systems, like lime shaft kilns with number of particles in the order of one million, still simplifications, like representing the lime stones by spheres, are necessary. Even then, computing times are significant. Very typical, the bottleneck in term of computing times is particle mechanics (neighbourhood search and contact resolution) and often not the thermochemical

processes. This allows for some freedom in selecting rather sophisticated methods to represent thermochemical conversion without influencing overall computing time to a large extend.

In summary, important research needs to make reacting DEM/CFD a standard engineering tool are:

- Fast neighbourhood and contact detection algorithms, especially for polydisperse granular assemblies with particles of complex shape,
- Improvement of contact heat transfer models for particles of complex shape,
- Reliable and fast particle-particle radiation models for moving polydisperse granular assemblies with particles of complex shape,
- Detailed single particle models, e.g. based on pore network simulations, to derive directional transport properties to formulate simpler single particle continuum models,
- Model reduction to provide fast single particle models based on ordinary differential equations,
- Methods to improve the spatial and directional representation of granular structure on the CFD side for the DEM/CFD porous medium approach for a more accurate prediction of the flow field,
- Effective methods which allow for a self-adaptive switch between locally resolved simulation of the particle shape on the CFD side and the porous media approach in the same computational domain,
- Validated gas phase combustion models which are able to describe the scale sensitivity of turbulence chemistry interaction as well as catalytic and quenching effects in the void space of the granular assembly,
- and, most important, experimental data sets for particle motion, gas phase velocity and homogeneous and heterogeneous reaction progress in high temperature granular assemblies to validate DEM/CFD simulations.

Note that many of these topics are currently addressed by the Collaborative Research Center 287 Bulk-Reaction, a larger-scale (10 million €) project funded by the German Research Foundation (DFG). For more details, see [67].

ACKNOWLEDGEMENTS

Funded by the Deutsche Forschungsgemeinschaft (DFG, German Research Foundation) – Project-ID 422037413 – TRR 287.

Gefördert durch die Deutsche Forschungsgemeinschaft (DFG) – Projektnummer 422037413 – TRR 287.

REFERENCES

- [1] P. A. Cundall and O. D. Strack, 1979, “A discrete numerical model for granular

- assemblies,” *Geotechnique*, vol. 29, pp. 47–65.
- [2] L. Zhan, C. Peng, B. Zhang, and W. Wu, 2021, “A surface mesh represented discrete element method (SMR-DEM) for particles of arbitrary shape,” *Powder Technol.*, vol. 377, pp. 760–779.
- [3] L. Fries, S. Antonyuk, S. Heinrich, and S. Palzer, 2011, “DEM-CFD modeling of a fluidized bed spray granulator,” *Chem. Eng. Sci.*, vol. 66, pp. 2340–2355.
- [4] L. Fries, S. Antonyuk, S. Heinrich, D. Dopfer, and S. Palzer, 2013, “Collision dynamics in fluidised bed granulators: A DEM-CFD study,” *Chem. Eng. Sci.*, vol. 86, pp. 108–123.
- [5] V. Salikov, S. Antonyuk, S. Heinrich, V. S. Sutkar, N. G. Deen, and J. A. M. Kuipers, 2015, “Characterization and CFD-DEM modelling of a prismatic spouted bed,” *Powder Technol.*, vol. 270, pp. 622–636.
- [6] N. G. Deen, M. V. S. Annaland, M. A. Van der Hoef, and J. A. M. Kuipers, 2007, “Review of discrete particle modeling of fluidized beds,” *Chem. Eng. Sci.*, vol. 62, pp. 28–44.
- [7] G. Lian, W. Zhong, and X. Liu, 2021, “CFD-DEM Investigation of Fuel Dispersion Behaviors in a 3D Fluidized Bed,” *Ind. Eng. Chem. Res.*, vol. 60, pp. 13272–13285.
- [8] Y. Guo and J. S. Curtis, 2015, “Discrete element method simulations for complex granular flows,” *Annu. Rev. Fluid Mech.*, vol. 47, pp. 21–46.
- [9] Z. Peng, E. Doroodchi, and B. Moghtaderi, 2020, “Heat transfer modelling in Discrete Element Method (DEM)-based simulations of thermal processes: Theory and model development,” *Prog. Energy Combust. Sci.*, vol. 79, p. 100847.
- [10] P. Kieckhefen, S. Pietsch, M. Dosta, and S. Heinrich, 2020, “Possibilities and limits of computational fluid dynamics–discrete element method simulations in process engineering: A review of recent advancements and future trends,” *Annu. Rev. Chem. Biomol. Eng.*, vol. 11, pp. 397–422.
- [11] S. Golshan, R. Sotudeh-Gharebagh, R. Zarghami, N. Mostoufi, B. Blais, and J. A. M. Kuipers, 2020, “Review and implementation of CFD-DEM applied to chemical process systems,” *Chem. Eng. Sci.*, vol. 221, p. 115646.
- [12] V. Scherer, S. Wirtz, B. Krause, and F. Wissing, 2017, “Simulation of reacting moving granular material in furnaces and boilers an overview on the capabilities of the discrete element method,” *Energy Procedia*, vol. 120, pp. 41–61.
- [13] A. Di Renzo, E. S. Napolitano, and F. P. Di Maio, 2021, “Coarse-Grain DEM Modelling in Fluidized Bed Simulation: A Review, 9, 279,” *Processes*, vol. 9, p. 279.
- [14] B. Peters, 1999, “Numerical simulation of the motion and combustion of granular material,” *Ind. Heat Eng.*, vol. 21, pp. 109–113.
- [15] B. Peters, M. Baniasadi, and M. Baniasadi, 2018, “The extended discrete element method (XDEM): An advanced approach to model blast furnace,” *Iron Ores and Iron Oxide Materials*, IntechOpen.
- [16] M. Mohseni, B. Peters, and M. Baniasadi, 2017, “Conversion analysis of a cylindrical biomass particle with a DEM-CFD coupling approach,” *Case Stud. Therm. Eng.*, vol. 10, pp. 343–356.
- [17] B. Peters, M. Baniasadi, M. Baniasadi, X. Besseron, A. E. Donoso, M. Mohseni, and G. Pozzetti, 2019, “XDEM multi-physics and multi-scale simulation technology: Review of DEM-CFD coupling, methodology and engineering applications,” *Particuology*, vol. 44, pp. 176–193.
- [18] X. Gao, J. Yu, L. Lu, and W. A. Rogers, 2021, “Coupling particle scale model and SuperDEM-CFD for multiscale simulation of biomass pyrolysis in a packed bed pyrolyzer,” *AIChE J.*, vol. 67, p. 17139.
- [19] S. Radl, T. Forgber, A. Aigner, and C. Kloss, 2015, “ParScale - An Open-Source Library for the Simulation of Intra-Particle Heat and Mass Transport Processes in Coupled Simulations,” *IVth International Conference on Particle-based Methods*, Barcelona, Spain.
- [20] K. Kuwagi, T. Takami, A.B. Alias, D. Rong, H. Takeda, S. Yanase, T. Kouchi, T. Hyakutake, K. Yokoyama, Y. Ohara, N. Takahashi, and N. Sugitsue, 2016, “Development of DEM-CFD Simulation of Combustion Flow in Incinerator with the Representative Particle Model,” *J. Chem. Eng. Jpn.*, vol. 49, pp. 425–434.
- [21] C. Spijker and H. Raupenstrauch, 2022, “CFD-DEM Modelling of shaft furnaces, using the volume fraction smoother approach,” *Conference on Modelling Fluid Flow*, Budapest, Hungary.
- [22] B. Krause, B. Liedmann, J. Wiese, S. Wirtz, and V. Scherer, 2015, “Coupled three dimensional DEM-CFD simulation of a lime shaft kiln - Calcination, particle movement and gas phase flow field,” *Chem. Eng. Sci.*, vol. 134, pp. 834–849.
- [23] T. Bluhm-Drenhaus, E. Simsek, S. Wirtz, and V. Scherer, 2010, “A coupled fluid dynamic-discrete element simulation of heat and mass transfer in a lime shaft kiln,” *Chem. Eng. Sci.*, vol. 65, pp. 2821–2834.
- [24] F. Wissing, S. Wirtz, and V. Scherer, 2017, “Simulating municipal solid waste incineration with a DEM/CFD method–

- Influences of waste properties, grate and furnace design,” *Fuel*, vol. 206, pp. 638–656.
- [25] V. Scherer, M. Mönnigmann, M. O. Berner, and F. Sudbrock, 2016, “Coupled DEM-CFD Simulation of Drying Wood Chips in a Rotary Drum - Baffle Design and Model Reduction,” *Fuel*, vol. 184, pp. 896-904.
- [26] J. Wiese, F. Wissing, D. Höhner, S. Wirtz, V. Scherer, U. Ley, and H.M. Behr, 2016, “DEM/CFD modeling of the fuel conversion in a pellet stove,” *Fuel Process. Technol.*, vol. 152, pp. 223–239.
- [27] F. Buss, S. Wirtz, and V. Scherer, 2020, “Simulation of a reacting agitated bed of straw pellets by a resolved coupled DEM/CFD method using a blocked-off approach,” *Int. J. Therm. Sci.*, vol. 152, p. 106332.
- [28] H. Kruggel-Emden, E. Simsek, S. Rickelt, S. Wirtz, and V. Scherer, 2007, “Review and extension of normal force models for the Discrete Element Method,” *Powder Technol.*, vol. 171, pp. 157–173.
- [29] H. Kruggel-Emden, S. Wirtz, and V. Scherer, 2008, “A study on tangential force laws applicable to the discrete element method (DEM) for materials with viscoelastic or plastic behavior,” *Chem. Eng. Sci.*, vol. 63, pp. 1523–1541.
- [30] E. Simsek, B. Brosch, S. Wirtz, V. Scherer, and F. Krüll, 2009, “Numerical simulation of grate firing systems using a coupled CFD/discrete element method (DEM),” *Powder Technol.*, vol. 193, pp. 266–273.
- [31] F. Elskamp, H. Kruggel-Emden, M. Hennig, and U. Teipel, 2017, “A strategy to determine DEM parameters for spherical and non-spherical particles,” *Granul. Matter*, vol. 19, pp. 1–13.
- [32] S. Luding, K. Manetsberger, and J. Müllers, 2005, “A discrete model for long time sintering,” *J. Mech. Phys. Solids*, vol. 53, pp. 455–491.
- [33] P. W. Cleary, 2010, “DEM prediction of industrial and geophysical particle flows,” *Particuology*, vol. 8, pp. 106–118.
- [34] H. Kruggel-Emden, M. Sturm, S. Wirtz, and V. Scherer, 2008, “Selection of an appropriate time integration scheme for the discrete element method (DEM),” *Comput. Chem. Eng.*, vol. 32, pp. 2263–2279.
- [35] X. Lin and T. NG, 1995, “Contact Detection Algorithms for Three-Dimensional Ellipsoids in Discrete Element Modelling,” *Int. J. Numer. Anal. Methods Geomech.*, vol. 19, pp. 653–659.
- [36] H. Ouadfel and L. Rothenburg, 1999, “An algorithm for detecting inter-ellipsoid contacts,” *Comput. Geotech.*, vol. 24, pp. 245–263.
- [37] P. W. Cleary and N. Stokes, 1997, “Efficient collision detection for three dimensional super-ellipsoid particles,” *8th International Computational Techniques and Applications Conference*, Adelaide, Australia.
- [38] P. W. Cleary and M. L. Sawley, 2002, “DEM modelling of industrial granular flows: 3D case studies and the effect of particle shape on hopper discharge,” *Appl. Math. Model.*, vol. 26, pp. 89–111.
- [39] S. Ji, S. Sun, and Y. Yan, 2015, “Discrete element modeling of rock materials with dilated polyhedral elements,” *Procedia Eng.*, vol. 102, pp. 1793–1802.
- [40] R. Deshpande, E. Illana Mahiques, S. Wirtz, and V. Scherer, accepted, “Resolving particle shape in DEM simulations from tabulated geometry information,” *Powder Technol.*
- [41] T. Weinhart, A. R. Thornton, S. Luding, and O. Bokhove, 2012, “From discrete particles to continuum fields near a boundary,” *Granul. Matter*, vol. 14, pp. 289–294.
- [42] A. Thornton, S. Luding, and O. Bokhove, 2012, “Modeling of particle size segregation: calibration using the discrete particle method,” *Int. J. Mod. Phys. C*, vol. 23, p. 1240014.
- [43] G. Stein, S. Wirtz, and V. Scherer, 2016, “Performance improvements of polydisperse DEM simulations using a loose octree approach,” *Parallel Comput. Road Exascale*, vol. 27, p. 53.
- [44] K. Dong, C. Wang, and A. Yu, 2015, “A novel method based on orientation discretization for discrete element modeling of non-spherical particles,” *Chem. Eng. Sci.*, vol. 126, pp. 500–516.
- [45] F. Sudbrock, 2014, “DEM/CFD Analyse der konvektiven Trocknung von bewegten Schüttungen,” *Dissertation Ruhr-Universität Bochum*.
- [46] F. Sudbrock, H. Kruggel-Emden, S. Wirtz, and V. Scherer, 2015, “Convective Drying of Agitated Silica Gel and Beech Wood Particle Beds—Experiments and Transient DEM-CFD Simulations,” *Dry. Technol.*, vol. 33, pp. 1808–1820.
- [47] W. L. Vargas and J. J. McCarthy, 2002, “Conductivity of granular media with stagnant interstitial fluids via thermal particle dynamics simulation,” *Int. J. Heat Mass Transf.*, vol. 45, pp. 4847–4856.
- [48] H. Hertz, 1881, “Über die Berührung fester elastischer Körper,” *J. Für Reine Angew. Mech.*, vol. 92, pp. 156–171.
- [49] T. Tsory, N. Ben-Jacob, T. Brosh, and A. Levy, 2013, “Thermal DEM–CFD modeling and simulation of heat transfer through packed bed,” *Powder Technol.*, vol. 244, pp. 52–60.
- [50] C. Joulin, J. Xiang, J.-P. Latham, C. Pain, and P. Salinas, 2020, “Capturing heat transfer for

- complex-shaped multibody contact problems, a new FDEM approach,” *Comput. Part. Mech.*, vol. 7, pp. 919–934.
- [51] S. Yagi and D. Kunii, 1957, “Studies on effective thermal conductivities in packed beds,” *AIChE J.*, vol. 3, pp. 373–381.
- [52] J. Gorewoda and V. Scherer, 2016, “Influence of carbonate decomposition on normal spectral radiative emittance in the context of oxyfuel combustion,” *Energy Fuels*, vol. 30, pp. 9752–9760.
- [53] G. J. Cheng and A. B. Yu, 2013, “Particle scale evaluation of the effective thermal conductivity from the structure of a packed bed: radiation heat transfer,” *Ind. Eng. Chem. Res.*, vol. 52, pp. 12202–12211.
- [54] H. Wu, N. Gui, X. Yang, J. Tu, and S. Jiang, 2016, “Effect of scale on the modeling of radiation heat transfer in packed pebble beds,” *Int. J. Heat Mass Transf.*, vol. 101, pp. 562–569.
- [55] L. Chen, C. Wang, M. Moscardini, M. Kamlah, and S. Liu, 2019, “A DEM-based heat transfer model for the evaluation of effective thermal conductivity of packed beds filled with stagnant fluid: Thermal contact theory and numerical simulation,” *Int. J. Heat Mass Transf.*, vol. 132, pp. 331–346.
- [56] J. Tausendschön and S. Radl, 2021, “Deep neural network-based heat radiation modelling between particles and between walls and particles,” *Int. J. Heat Mass Transf.*, vol. 177, p. 121557.
- [57] J. Wiese, 2015, “Experimentelle und numerische Untersuchungen an Holzpelletfeuerungen,” *Dissertation Ruhr-Universität Bochum*.
- [58] S. Ergun, 1952, “Fluid flow through packed columns,” *Chem Eng Prog*, vol. 48, pp. 89–94.
- [59] R. Di Felice, 1994, “The voidage function for fluid-particle interaction systems,” *Int. J. Multiph. Flow*, vol. 20, pp. 153–159.
- [60] J. E. Hilton and P. W. Cleary, 2011, “The influence of particle shape on flow modes in pneumatic conveying,” *Chem. Eng. Sci.*, vol. 66, pp. 231–240.
- [61] Z. Y. Zhou, D. Pinson, R. P. Zou, and A. B. Yu, 2011, “Discrete particle simulation of gas fluidization of ellipsoidal particles,” *Chem. Eng. Sci.*, vol. 66, pp. 6128–6145.
- [62] H. Kruggel-Emden and T. Oschmann, 2014, “Numerical study of rope formation and dispersion of non-spherical particles during pneumatic conveying in a pipe bend,” *Powder Technol.*, vol. 268, pp. 219–236.
- [63] B. G. M. van Wachem, V. Chéron, and F. Evrard, 2022, “Discrete element modelling of non-spherical particles in turbulent gas-solid flows,” *Conference on Modelling Fluid Flow*, Budapest, Hungary.
- [64] E. Illana Mahiques, M. Brömmer, S. Wirtz, and V. Scherer, 2022, “Local flow resolution with the Blocked-Off method in DEM-CFD: Gaseous fuel jet dispersion and combustion in a particle assembly,” *Conference on Modelling Fluid Flow*, Budapest, Hungary.
- [65] A. Alkhalaf, H. A. Refaey, N. Al-durobi, and E. Specht, 2018, “Influence of contact point treatment on the cross flow mixing in a simple cubic packed bed: CFD simulation and experimental validation,” *Granul. Matter*, vol. 20, p. 22.
- [66] B. Krause *et al.*, 2017, “3D-DEM-CFD simulation of heat and mass transfer, gas combustion and calcination in an intermittent operating lime shaft kiln,” *Int. J. Therm. Sci.*, vol. 117, pp. 121–135.
- [67] “Bulk-Reaction.” <https://bulk-reaction.de/> (accessed Jun. 13, 2022).